Brillouin microscopy for the evaluation of hair micromechanics and effect of bleaching

N. Correa[1], M. Alunni Cardinali[2], M. Bailey[1], D. Fioretto[2], P.D.A. Pudney[3], F. Palombo[1*]

[1] *School of Physics, University of Exeter, Exeter, UK*

[2] *Department of Physics and Geology, University of Perugia, Perugia, Italy*

[3] *Unilever R&D Port Sunlight, Quarry Road East, Bebington, Wirral, CH63 3JW*

**Corresponding author; e-mail: f.palombo@exeter.ac.uk*

Abstract

Brillouin microscopy is a new form of optical elastography and an emerging technique in mechanobiology and biomedical physics. It was applied here to map the viscoelastic properties of human hair and to determine the effect of bleaching on hair properties. For hair samples, longitudinal measurements (i.e. along the fibre axis) revealed peaks at 18.7 GHz and 20.7 GHz at the location of the cuticle and cortex, respectively. For hair treated with a bleaching agent, the frequency shifts for the cuticle and cortex were 19.7 GHz and 21.0 GHz, respectively, suggesting that bleaching increases the cuticle modulus and - to a minor extent - the cortex modulus. These results demonstrate the capability of Brillouin spectroscopy to address questions on micromechanical properties of hair and to validate the effect of applied treatments.

Keywords: fibres, matrix, viscoelasticity, biomechanics, Young's modulus, elasticity tensor.

1. Introduction

Hair is a complex system formed by several morphological components that act as a unit. It can be divided into two major structures: the follicle and the fibre. The part that we see above the skin corresponds to the hair fibre, while the hidden part inside the skin is the hair follicle. The latter component is the living part of the hair and it generates the hair fibre. The hair fibre is a non-living structure, and its elastic properties can be changed by ageing, environmental factors, as well as under the influence of water, temperature and reagents such as those used in cosmetic treatments.[1-3]

The hair shaft has a diameter of approximately 50-100 μm and, although its function in humans has diminished relative to other mammals, it does help to protect the scalp from mechanical abrasion, sunburn and provides thermoregulation. It also has strong cultural significance as it is an area where appearance can be varied. People spend considerable effort cleaning, colouring and styling their hair, and hence it is of significant importance to the cosmetic industry. It is divided into three main morphological constituents: cuticle, cortex and, in some cases, medulla (Figure 1).[4,5]

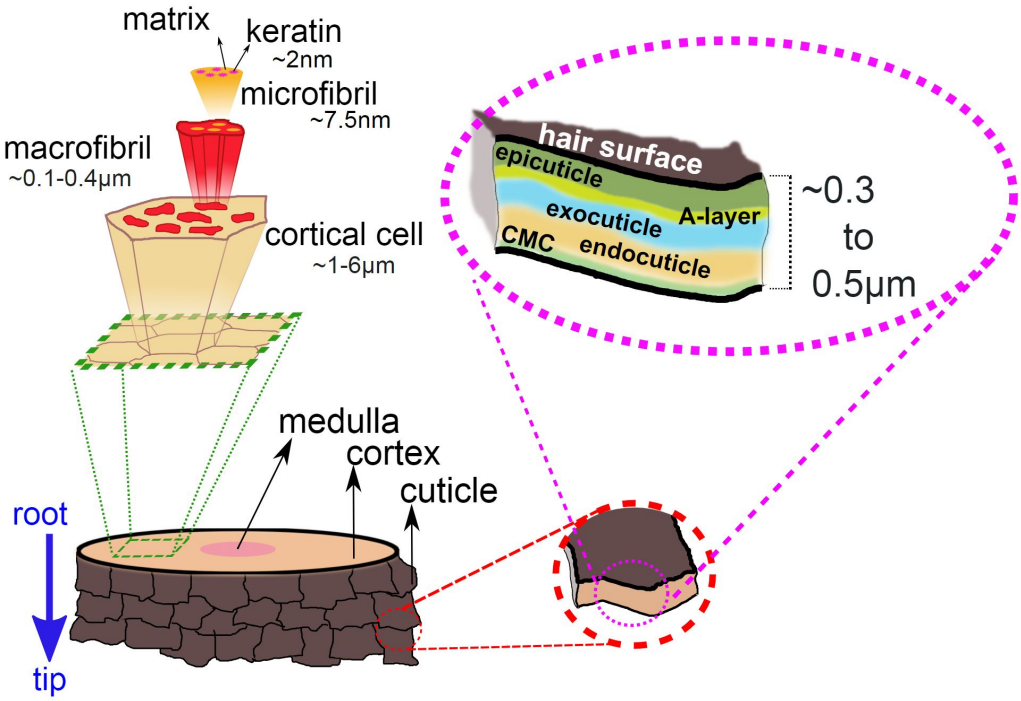

Figure 1. Schematic representation of the hair shaft, with a close-up view of a cuticle scale and cortex. The different layers that form the cuticle scale and the different structures that form the cortex are illustrated.

The cuticle is a barrier that protects the cortex from external environmental damage and it only represents 10% (dry weight) of the whole hair fibre.[6] It primarily consists of keratin in β-sheet conformation with a high amount of sulphur–sulphur bonds. It comprises 6 to 10 layers of overlapping scales, whose shape and orientation limit the friction between hair fibres. Each one of these cuticle scales is a complex substructure, with different layers. The outermost layer is the epicuticle, which provides lubricity to the hair and represents the first line of defence against external aggressions. Immediately below is the A-layer, which provides structural strength and rigidity to the cuticle. The next layers are the exocuticle, also called B-layer, and finally the endocuticle. To hold cuticle scales together, a non-keratinous protein layer called the cellular matrix complex (CMC) acts as intercellular cement.

The cortex represents the major part of the hair mass (>90% dry weight).[7] It is composed of cortical cells and the CMC. Cortical cells are tightly packed with macrofibrils, which have a hierarchical structure starting from keratin in a α-helical fold. This builds up through intermediate filaments and microfibrils. Surrounding the keratin is the matrix which mainly consists of keratin associated proteins (KAPs).[8] Finally, in some cases (e.g. thick hair), the medulla is found in the core of the hair fibre.[9] It may be continuous, discontinuous or entirely absent. It is believed that its contribution to the mechanical properties of the hair fibre is negligible.[3]

Cosmetic science is constantly researching new ways to develop new hair products to treat damaged hair. Different techniques have been used to study the changes induced by different hair products and treatments commonly employed. Atomic force microscopy (AFM),[10] optical coherence tomography (OCT), [11-13] Raman spectroscopy,[14,15] differential scanning calorimetry (DSC),[16-19] and scanning electron microscopy (SEM) are the techniques generally employed to characterise the effects of products and treatments. Brillouin spectroscopy is a significant addition to this list as it is non-destructive, all-optical

and contactless, and gives access to mechanical properties (compressibility, viscosity) on a micro-scale via excitation of spontaneous acoustic waves or phonons.

Brillouin microscopy is an emerging technique in biophotonics that has demonstrated potential for live cell mechanics and biomedical applications.[20-22] Brillouin spectroscopy probes light scattered by periodic fluctuations in density that occur in materials by virtue of thermally excited acoustic waves or phonons.[23] When combined with confocal microscopy, Brillouin measurements provide maps of frequency shifts which is related to the longitudinal storage modulus (or stiffness) and maps of linewidth which relates to the longitudinal loss modulus (or apparent viscosity). In the case of fibrous samples, changing the scattering geometry enables different orientations of the scattering vector ($\boldsymbol{q}$) to be selected, thereby probing the anisotropy in acoustic wave velocity and hence in mechanical properties for the different directions of the fibre.[24]

Previously, the Brillouin spectra of horse hair have been examined by Randall and Vaughan,[25] and then by Koski[26] showing a shift of ca. 18 GHz for horse white hair measured with a laser wavelength of 532.15 nm and 180° scattering angle. Koski *et al.* have used a confocal Brillouin microscope to investigate the elastic properties of spider silks by fully characterising the stiffness tensor and elastic moduli.[27] In our work on wool, which – similarly to hair – is mainly composed of the structural protein keratin, some of which are stabilized by disulphide bonds, we have observed a peak at 19 GHz measured at 532 nm for 180° scattering angle and in the transverse direction (radial orientation of $\boldsymbol{q}$) to the fibre axis.[28] A recent study by Elsayad *et al.* has investigated the mechanical properties of cellulose fibres in light of their anisotropy and the difference between the longitudinal modulus along the fibre axis and that perpendicular to it.[29] In the present study, high-contrast Brillouin microscopy was employed to map the viscoelastic properties of human hair and to investigate the effect of bleaching. The measurements were conducted with the scattering vector along the hair shaft axis and hence they yielded a longitudinal modulus parallel to the hair axis ($M_{\parallel}$).

2. Materials and Methods

2.1 Sample preparation

Samples of virgin and bleached hair were used in this study. Virgin hair was provided by Unilever supplied from International Hair importers and was European natural white. A bleaching mixture containing L'Oréal Platine Precision bleach powder and 9% Excel cream peroxide was prepared in a 1:2 ratio by weight. The mixture was applied to each hair strand using a tinting brush and left to develop for 30 minutes. The hair strands were then rinsed for 2 minutes and left to dry in air for 2 hours. Following this treatment, a second bleach cream mixture was applied to the bleached hair. After leaving it for 30 minutes, the hair strands were washed using a base shampoo (17.10 wt. % sodium lauryl sulphate, 5.33 wt. % cocoamido-propyl betaine, 0.40 wt. % DMDM hydantoin, 1.40 wt. % sodium chloride, in water) and air-dried.

A low-viscosity epoxy resin, SPURR (EM0300-1KT; Sigma-Aldrich), was used as the embedding medium. SPURR is a hydrophobic resin which was employed here to obtain small blocks, of approximately 9 mm^3 size, containing hair samples that were cut perpendicular to the hair shaft axis. For comparative purposes, virgin and bleached hair were also embedded in Agar100 and in optical cutting temperature medium and cryosectioned (to 30 μm thickness), giving a total of 6 specimens; data showed no change in Brillouin parameters compared to the results presented hereafter. Prior to

the Brillouin measurements, white light images were acquired for each sample using a Leica microscope with a 20× objective.

2.1 Brillouin microscopy

Micro-Brillouin maps of the hair specimens were measured using a high-contrast (3+3)-pass tandem Fabry-Pérot interferometer (TFP-2 HC) coupled to a customized JRS Scientific Instruments confocal microscope (CM-1),[30] as shown in Figure 2. The laser source employed was a solid state single mode 532 nm laser (Excelsior Diode Pumped Solid State, DPSS) with a power ranging between 0.4 and 6 mW for bleached and virgin hair, respectively. These values were measured at the objective's back focal plane. The objective utilised for illumination and collection was a Mitutoyo MPlan Apo 20×, NA 0.42 with a very long (20 mm) working distance. The system had a nominal resolution of 2 µm (lateral resolution) and 8 µm (axial resolution). The backscattered light was analysed by the spectrometer and detected by a single-photon avalanche diode (SPAD).

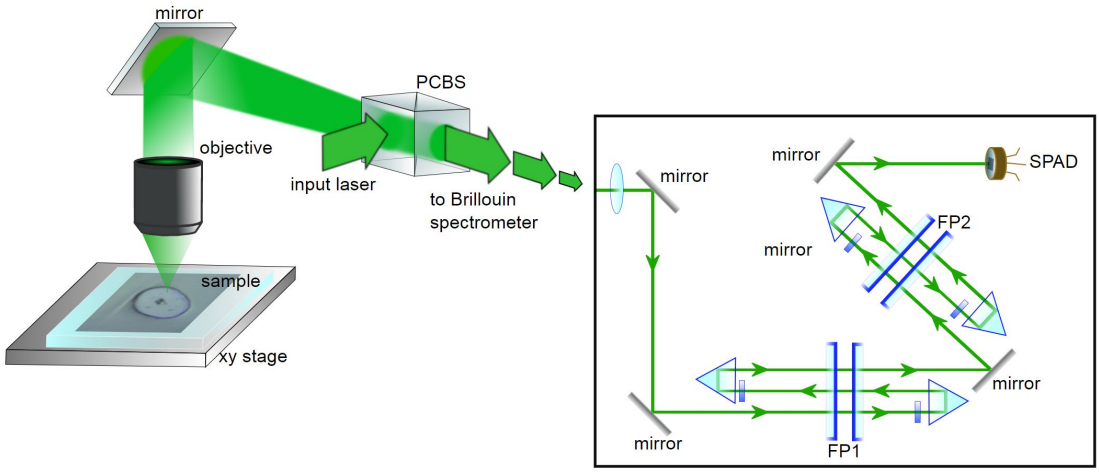

Figure 2. Schematic diagram of the Brillouin microscope consisting of a (3+3)-pass tandem Fabry-Pérot interferometer with two etalons (FP1 and FP2) and a single-photon avalanche diode (SPAD) detector, coupled to a customized JRS Scientific Instruments confocal microscope. PCBS: polarizing cube beam splitter.

The Brillouin spectra were acquired using a free spectral range of 40 GHz. Exposure times of 1 minute for virgin hair and 2 minutes for bleached hair were used in order to achieve a good signal-to-noise ratio for full lineshape analysis.

Maps were obtained by point-scanning the laser spot across 2D regions of the samples, with each point corresponding to a Brillouin spectrum from a specific location within the sample. Data acquisition was performed using GHOST software.

Each Brillouin spectrum presents peaks at a frequency shift from the Rayleigh peak which is given by the equation: $\nu_B = \pm\frac{2n}{\lambda}V$, where $\frac{2n}{\lambda}$ stems from the scattering wave vector $q = 2nk$, with n being the material's refractive index, and V is the acoustic wave velocity. In the case of a 180° scattering geometry such as the one used in these measurements, the incident light wave vector is $k = \frac{2\pi}{\lambda}$, where λ is the incident light wavelength. The acoustic wave velocity V derived from the peak frequency shift

is related to the longitudinal storage modulus, $M' = \rho V^2$, where ρ is the material's density. The longitudinal loss modulus can be obtained from the linewidth of the Brillouin peak Γ_B through $M'' = \rho V^2 \frac{\Gamma_B}{\nu_B}$.

Fit analysis was applied to all the Brillouin spectra in the range 17 to 23 GHz, both Stokes and anti-Stokes sides, and average parameters were calculated. The Brillouin spectra of hair presented doublet peaks, which required simultaneous fit of two peaks for each of the Stokes and anti-Stokes parts of the spectrum. The curve fitting routine was written in Fortran77 and was based on a damped harmonic oscillator (DHO) model including convolution with an instrumental Gaussian function.[20] Various spurious effects can cause peak broadening, such as illumination/collection geometry, absorption in strongly scattering media, multiple scattering, and the use of high NA objectives (enabling a range of q values).[31,32] In this work, a backscattering geometry was employed together with a small NA objective, thus minimizing the effect of spurious Brillouin line broadening. The computed parameters of each DHO function are: peak intensity (I_B), frequency shift (ν_B), linewidth (Γ_B) and tan(δ), i.e. the ratio of imaginary-to-real part of the longitudinal modulus, given by the ratio of linewidth-to-frequency shift. Brillouin maps were obtained for each of these parameters, which respectively reflect the distribution of density (for samples of uniform thickness as in this case),[33] micro-compressibility, apparent viscosity and acoustic wave attenuation across the scanned region of the sample. An overall intensity map was obtained by plotting the sum of the two peaks intensities derived from fit analysis.

3. Results

Figure 3 shows the results of the measurements performed on a virgin hair embedded in SPURR (see Figure SI-1 in Supplementary Material). A Brillouin map plotting the overall intensity of the spectrum in the range 17–23 GHz is shown in Figure 3b. Single spectral profiles for the locations corresponding to (1) cuticle, (2) cuticle-cortex interface, and (3) cortex are presented together with the fit results (Figure 3c).

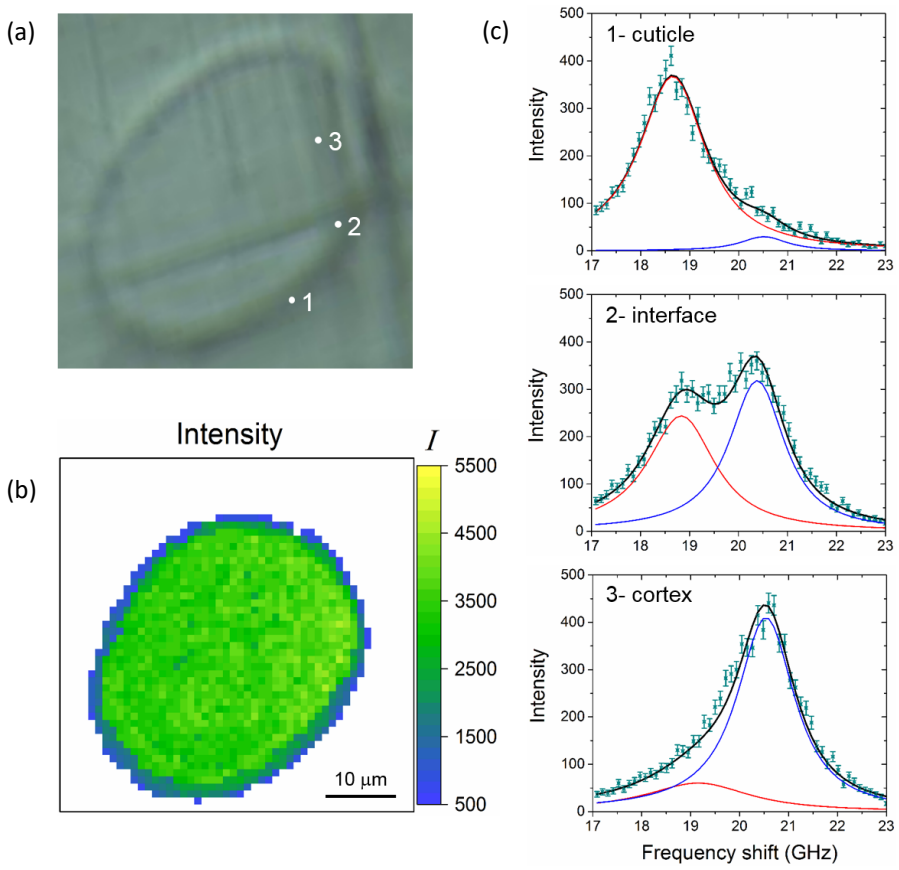

Figure 3. (a) White light image of a virgin hair. Dots denote the locations from which Brillouin spectra were extracted. (b) Image showing the distribution of intensity (overall intensity map) across the scanned area of 50 × 50 µm^2 where Brillouin spectra were acquired using a 1 µm step-size. (c) Fit results for the anti-Stokes peaks of the Brillouin spectra extracted from the locations 1-cuticle, 2-interface and 3-cortex in (a). Symbols indicate the experimental data, whilst the black line is the result of a least-square fit to two damped harmonic oscillator functions, one at low frequency (red line) and one at high frequency (blue line). Error bars denote the standard error, i.e. square root of number of counts.

The cuticle and cortex are essentially represented by single peaks at distinct frequency shifts, cuticle: 18.8 GHz and cortex: 20.6 GHz (Figure 3c), whilst the interface (2) is characterised by the presence of two peaks with fairly similar intensity. The spectrum of the cuticle (1) is plausibly not a 'pure' spectrum, as the cuticle is thinner than the actual spatial resolution in these measurements. However its frequency shift, ca. 19 GHz, is similar to that of other protein structures, namely those made of collagen,[24,34] hence the peak (red line in 1) mainly reflects the keratin-rich composition of the cuticle. The spectrum of the cortex (3) drawn from inside the hair shows a large contribution from a high frequency component, at ca. 21 GHz, plausibly related to the intermediate filaments in the cortical cells, and a minor contribution at approximately 19 GHz that may be indicative of the surrounding matrix made of mainly keratin associated proteins (KAPs).[8] The observed shift of the low frequency component (red line in 1, 2 and 3) is very similar to that of type-I collagen fibres of the extracellular matrix, 18.9 GHz.[24]

Maps of the Brillouin peak intensity, frequency shift, linewidth and tan(δ) for each of the two major hair components, cuticle and cortex, derived from fit analysis are reported in Figure 4.

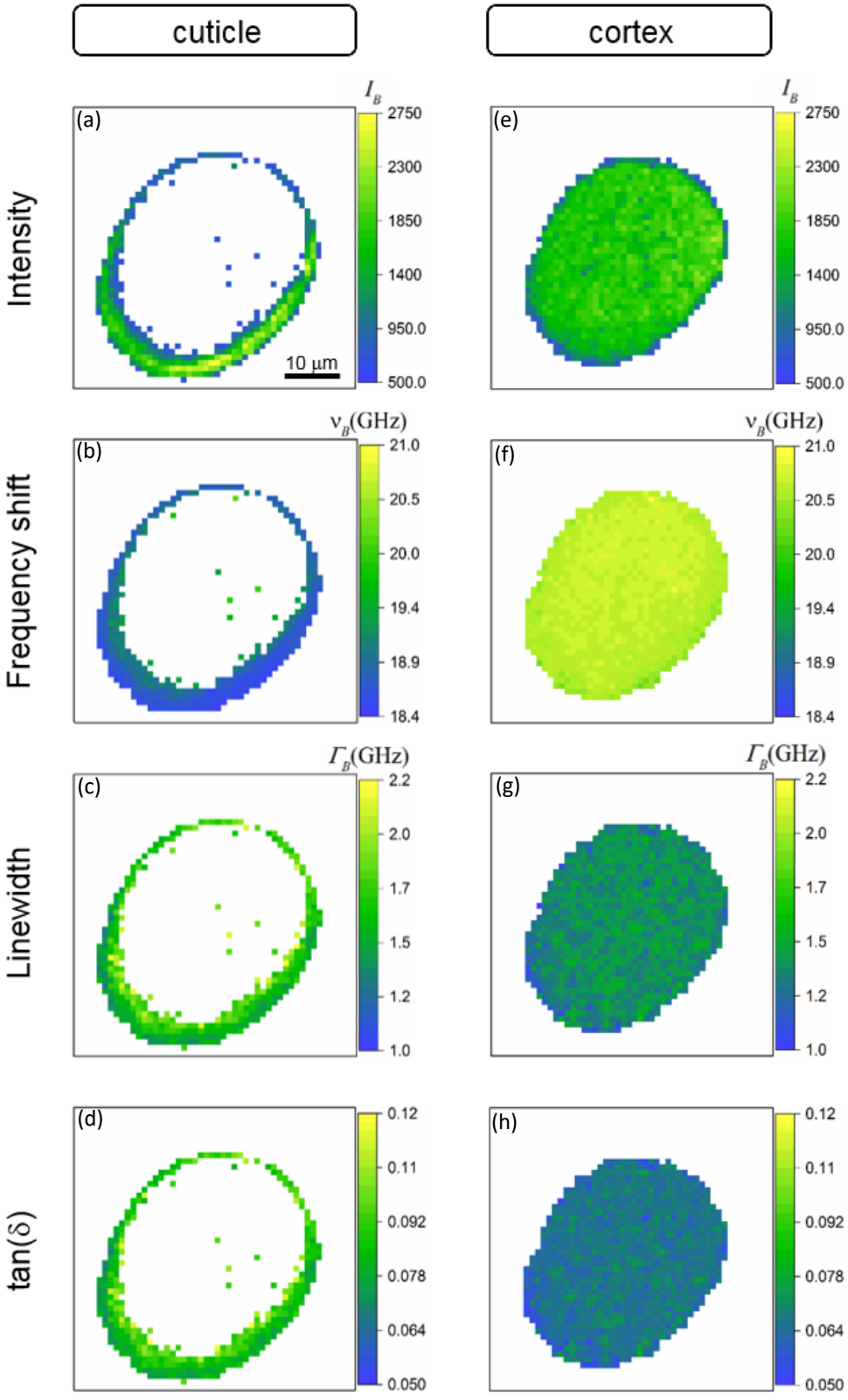

Figure 4. Virgin hair. Brillouin maps are based on DHO fit results: (a, e) peak intensity, (b, f) frequency shift, (c, g) linewidth, and (d, h) tan(δ) for (left panels) the cuticle and (right panels) cortex.

Intensity maps are complementary images whereby the cuticle is denoted by a ring-shaped region (Figure 4a) and the cortex is a well-defined round region (Figure 4e) which represents the major

component of the hair. The cuticle region presents a main Brillouin peak at lower frequency (Figure 4b) than that of the cortex (Figure 4f); however, the linewidth is broader (Figure 4c vs g) indicating a higher apparent viscosity. This is reflected in the attenuation of the acoustic wave expressed by the quantity tan(δ), which is more pronounced (by approximately 30%) in the cuticle (Figure 4d) than the cortex (Figure 4h), with a gradient in attenuation that increases from the outer to the inner cuticle, whilst the cortex appears more uniform.

Figures 5 and 6 show the results for bleached hair.

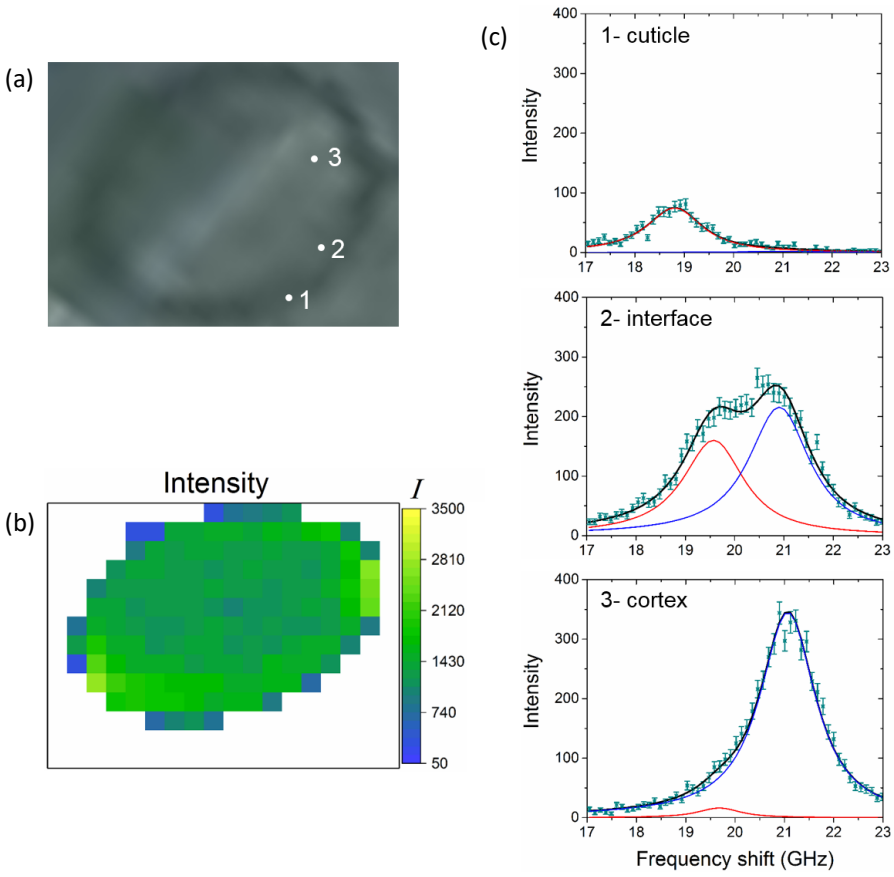

Figure 5. (a) White light image of a bleached hair. (b) Brillouin intensity map: 80 × 60 μm^2 acquired with a 5 μm step-size. (c) Fit results for the anti-Stokes peaks of the Brillouin spectra extracted from the map, at points 1-cuticle, 2-interface and 3-cortex in (a). Symbols, experimental data; black line, result of a least-square fit to two damped harmonic oscillator functions: red line, low frequency peak, and blue line, high frequency peak; error bars, standard error, i.e. square root of number of counts.

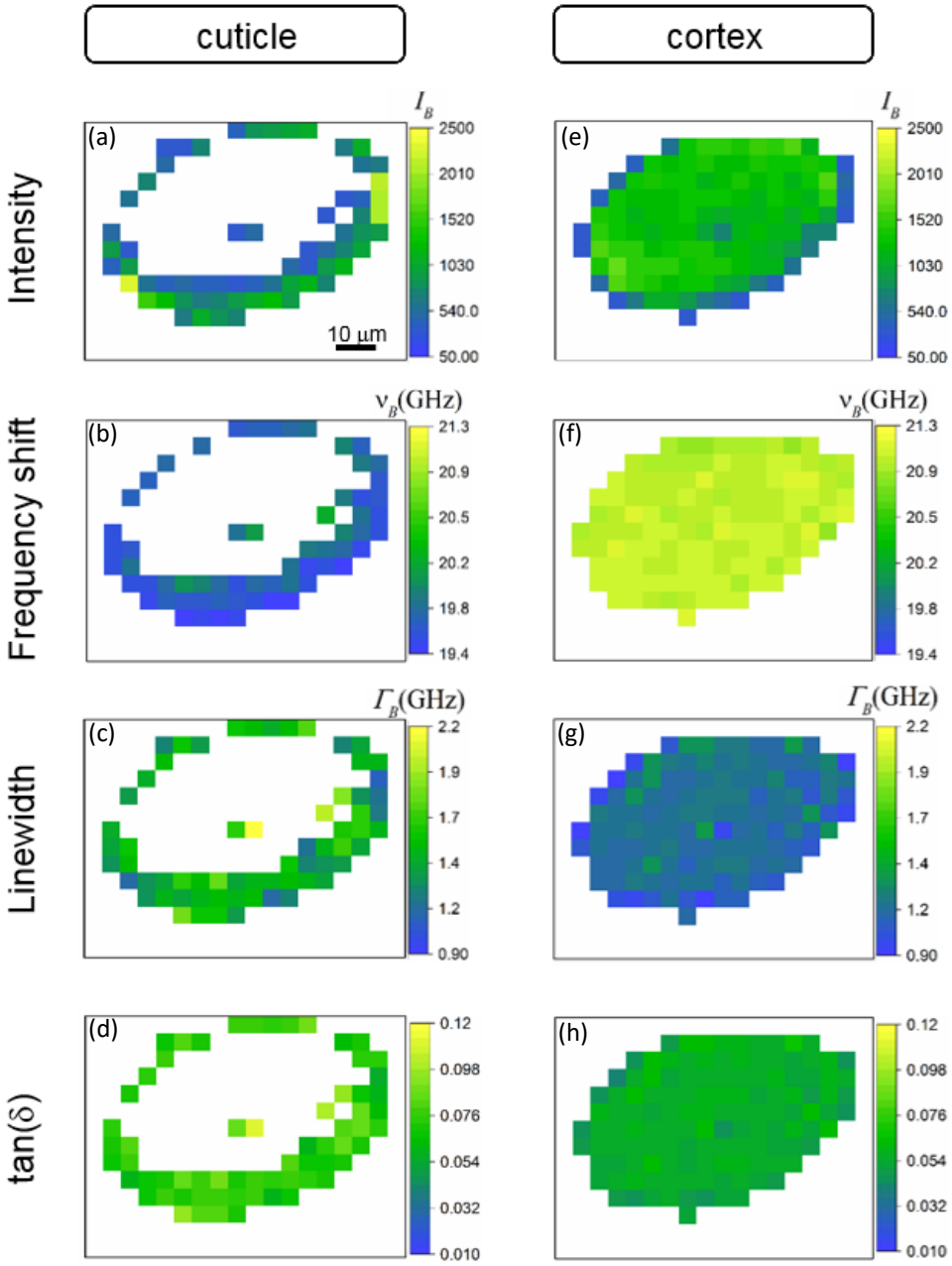

Figure 6. Bleached hair. Brillouin maps are based on DHO fit results: (a, e) peak intensity, (b, f) frequency shift, (c, g) linewidth and (d, h) tan(δ) for (left panels) the cuticle and (right panels) cortex.

Fit results listed in Table I show that the frequency shifts are 18.7 GHz for the cuticle of virgin hair and 19.7 GHz for the cuticle of bleached hair, whilst for the cortex the values are 20.7 GHz for virgin hair and 21 GHz for bleached hair. This result shows that bleaching causes a sizeable increase in frequency shift for the cuticle, 1 GHz, and a smaller increase, 0.3 GHz, for the cortex. By introducing the values of density (1.3429 g cm^{-3} average[35]) and refractive index (1.54 for cuticle and 1.56 for cortex[36]), a storage modulus $M_{\parallel}$ of 14.1 GPa for the cuticle of virgin hair and 15.4 GPa for the cuticle of bleached hair is obtained, whilst for the cortex the values are 16.6 GPa for virgin hair and 17.1 GPa for bleached hair. The effect of bleaching is therefore to increase the storage modulus of hair (assuming the density remains constant, as it is the case for the refractive index[36]) and this is more pronounced in the cuticle, i.e. the outer layer, than cortex.

The Brillouin linewidth, which is ca. 30% larger for the cuticle than the cortex, is found to reduce for both structures upon bleaching, suggesting that in bleached hair the apparent viscosity is lower than in virgin hair plausibly due to a change in the proteins. The loss modulus also decreases due to bleaching (Table I).

In terms of tan(δ), values are comparable however for both cuticle and cortex, the bleached hair presents smaller attenuation (0.08 and 0.059; Fig. 6d, h) than the virgin hair (0.088 and 0.067) indicating reduced apparent viscosity.

Table I. Brillouin-derived longitudinal parameters of hair samples.

	Virgin hair		Bleached hair	
Parameter	**Cuticle**	**Cortex**	**Cuticle**	**Cortex**
Frequency shift (GHz)	18.7 ± 0.2	20.7 ± 0.6	19.7 ± 0.2	21.0 ± 0.1
Linewidth (GHz)	1.8 ± 0.5	1.4 ± 0.4	1.6 ± 0.2	1.3 ± 0.1
tan(δ)	0.088 ± 0.010	0.067 ± 0.035	0.080 ± 0.010	0.059 ± 0.006
Storage modulus (GPa)	14.1 ± 0.3	16.6 ± 0.5	15.4 ± 0.4	17.1 ± 0.1
Loss modulus (GPa)	1.3 ± 0.4	1.1 ± 0.3	1.2 ± 0.2	1.0 ± 0.1

Errors are average errors derived from fit analysis of Stokes and anti-Stokes peaks of the Brillouin spectra.

4. Discussion

Here we presented the first study of human hair in both virgin and bleached forms using high-contrast Brillouin microscopy. Measurements were performed on virgin and bleached hair samples embedded in a low-viscosity hydrophobic epoxy resin, SPURR. Results from these measurements (Figure 5) show that Brillouin spectroscopy is capable of discriminating between cuticle and cortex in hair samples. The cuticle presents a Brillouin peak at 18.7 GHz which denotes a protein (keratin)-rich layer. The cortex presents a major component at higher frequency, 21 GHz, the intermediate filaments in the cortical cells, and a minor contribution at approximately 19 GHz that may be related to the surrounding matrix. Difference in peak frequency shift between these two components is of the order of 2 GHz, which is appreciable in terms of viscoelastic properties as revealed by Brillouin spectroscopy.

Previous work conducted on virgin (not white) Japanese hair has shown that cuticle and cortex differ markedly in terms of torsional and Young's moduli, with cuticle found to be approximately 4 times more rigid than cortex.[37] The Young's modulus of whole hair has been given as 9.49 GPa, that of cortex as 5.55 GPa and for cuticle 19.85 GPa. Also, the ratio of Young's modulus to rigidity modulus is very large (E/G = 11.94), much higher than that of a homogeneous material, hence reflecting the anisotropy

with respect to stress because cuticle and cortex are composite materials with complex internal structures. The marked difference in Young's modulus between cortex and cuticle in not reflected in our Brillouin results, which show that the storage modulus for cortex is larger than that of cuticle: 16.6 GPa and 14.1 GPa, respectively. Smaller changes in Brillouin-derived modulus than those in quasi-static measurements and AFM-derived Young's modulus have already been reported for other materials, e.g. collagen fibres,[38] cellulose fibres[29] and gelatin hydrogels,[39] and attributed to different spatio-temporal scales and different types of modulus probed by the two techniques.

We also observed here that the frequency shifts of cuticle and cortex increase upon bleaching (Table I), especially for the cuticle i.e. the outer layer, as it can be expected, which is reflected in an increase in storage modulus. In a previous report,[40] bleach treatment which involves the oxidative attack on the disulphide bonds of hair keratin has been found to increase the modulus of the fibre at low humidity, such as the condition used in this study. Oxidative damage increases the tensile modulus and torsional modulus (effect on cuticle). It has also been observed that bleaching has a larger effect on torsional properties than on tensile properties, with an increase in torsional modulus as a function of the number of bleach treatments. These changes are in line with our observation of increased storage modulus of both cortex and cuticle upon bleaching (effect on matrix and especially cuticle).

An increased storage modulus in correspondence to a reduced loss modulus (Table I) has previously been reported for solid-like (low hydration) biological tissues and interpreted based on a structural relaxation mechanism.[20] Here the change in storage and loss moduli is driven by a change in proteins due to the oxidative reaction. Further work is needed to clarify the extent to which this contributes a change in architecture, biophysical and biomechanical properties of the hair.

These results demonstrate the ability of Brillouin microscopy to map viscoelastic properties of hair and the effect of bleaching, the classical model for hair damage in industry. It is 'baseline' against which effects of treatments are judged. Brillouin microscopy shows that it can extract finer details on the hair substructures to what is known, without further damage or external loading applied to the sample. This method will allow precise location of the effect of treatment across the hair structure at a level not presently available, whether that be to damaged hair fibres or virgin hair. It a promising technique for studying hair further.

Acknowledgements

The authors would like to thank Dr Christian Hacker at the University of Exeter for the resin-embedded sample preparation. This work was supported by the UK Engineering and Physical Sciences Research Council (EPSRC) through an IAA Impact and Knowledge Exchange Award (EP/R511699/1) jointly with Unilever. FP acknowledges support by the EPSRC (EP/M028739/1) and jointly Cancer Research UK (NS/A000063/1). NC was also supported by the EU COST Action BioBrillouin (CA16124) for a Short Term Scientific Mission at DF's lab.

Author contributions

FP, DF and PDAP conceived, designed and supervised the project. NC, MAC and MB performed all experiments. NC and DF processed and analysed the data. FP and PDAP helped with discussion of the results. NC, FP, DF and PDAP wrote the manuscript with input from all other authors.

Author information

Supporting information is available online.

Reprints and permissions information is available at

The authors declare no competing interests in relation to this work.

The data that support the findings of this study are available from the corresponding author upon reasonable request.

References

1 Astbury W. T. and Woods H. J. The X-Ray Interpretation of the Structure and Elastic Properties of Hair Keratin. *Nature* **126**, 913-914 (1930).

2 Bhushan B. and LaTorre C. Structural, Nanomechanical, and Nanotribological Characterization of Human Hair Using Atomic Force Microscopy and Nanoindentation. In *Nanotribology and Nanomechanics*, 1325-1485 (Springer, Berlin, Heidelberg, 2008).

3 Bhushan B. Nanoscale characterization of human hair and hair conditioners. *Progress in Materials Science* **53**, 585-710 (2008).

4 Cruz C. F., Costa C., Gomes A. C., Matamá T. and Cavaco-Paulo A. Human Hair and the Impact of Cosmetic Procedures: A Review on Cleansing and Shape-Modulating Cosmetics. *Cosmetics* **3**, 26 (2016).

5 Cloete E., Khumalo N. P., Van Wyk J. C. and Ngoepe M. N. Systems Approach to Human Hair Fibers: Interdependence Between Physical, Mechanical, Biochemical and Geometric Properties of Natural Healthy Hair. *Frontiers in Physiology* **10**, 112 (2019).

6 Benzarti M., Tkaya M. B., Mattei C. P. and Zahouani H. Hair mechanical properties depending on age and origin. *World Academy of Science, Engineering and Technology* **74**, 471-477 (2011).

7 Benzarti M., Pailler-Mattei C., Jamart J. and Zahouani H. The Effect of Hydration on the Mechanical Behaviour of Hair. *Experimental Mechanics* **54**, 1411-1419 (2014).

8 Es'haghian S. *et al.* In vivo volumetric quantitative micro-elastography of human skin. *Biomedical Optics Express* **8**, 2458-2471 (2017).

9 Howlett R. A. *et al.* Peripheral oxygen transport and utilization in rats following continued selective breeding for endurance running capacity. *Journal of Applied Physiology* **106**, 1819-1825 (2009).

10 Samanta A. *et al.* Nanomechanical responses of human hair. *Journal of the Mechanical Behavior of Biomedical Materials* **56**, 229-248 (2016).

11 Choi W. J., Min G., Lee B. H., Pi L.-Q. and Lee W.-S. Qualitative investigation of fresh human scalp hair with full-field optical coherence tomography. *Journal of Biomedical Optics* **17**, 036010 (2012).

12 Tsugita T. and Iwai T. Optical coherence tomography using images of hair structure and dyes penetrating into the hair. *Skin Research and Technology* **20**, 389-398 (2014).

13 Arumugam K., Wang Y., Hardy L. L., MacNicol M. C. and MacNicol A. M. Enforcing temporal control of maternal mRNA translation during oocyte cell-cycle progression. *The EMBO Journal* **29**, 387-397 (2010).

14 Pudney P. D. *et al.* Confocal Raman spectroscopy of whole hairs. *Applied Spectroscopy* **67**, 1408-1416 (2013).

15 Kuzuhara A., Fujiwara N. and Hori T. Analysis of internal structure changes in black human hair keratin fibers with aging using Raman spectroscopy. *Biopolymers* **87**, 134-140 (2007).

16 Wortmann F. J., Stapels M., Elliott R. and Chandra L. The effect of water on the glass transition of human hair. *Biopolymers* **81**, 371-375 (2006).

17 Jinks I., Paul P. and Wortmann F. J. The effects of esterification on the humidity-dependent glass transition of human hair. *Thermochimica Acta* **614**, 33-36 (2015).
18 Wortmann F. J., Wortmann G. and Popescu C. Kinetics of the changes imparted to the main structural components of human hair by thermal treatment. *Thermochimica Acta* **661**, 78-83 (2018).
19 Wortmann F. J., Wortmann G. and Popescu C. Linear and nonlinear relations between DSC parameters and elastic moduli for chemically and thermally treated human hair. *Journal of Thermal Analysis and Calorimetry*, **140**, 2171-2178 (2019).
20 Palombo F. and Fioretto D. Brillouin Light Scattering: Applications in Biomedical Sciences. *Chemical Reviews* **119**, 7833-7847 (2019).
21 Prevedel R., Diz-Muñoz A., Ruocco G. and Antonacci G. Brillouin microscopy: an emerging tool for mechanobiology. *Nature Methods* **16**, 969-977 (2019).
22 Elsayad K., Polakova S. and Gregan J. Probing Mechanical Properties in Biology Using Brillouin Microscopy. *Trends in Cell Biology* **29**, 608-611 (2019).
23 Brillouin L. Diffusion de la lumière et des rayons X par un corps transparent homogène. *Annales de Physique* **9**, 88-122 (1922).
24 Palombo F. *et al.* Biomechanics of fibrous proteins of the extracellular matrix studied by Brillouin scattering. *Journal of the Royal Society Interface* **11**, 12 (2014).
25 Randall J., Vaughan J. M. and Cusak S. Brillouin Scattering in Systems of Biological Significance [and Discussion]. *Philosophical Transactions of the Royal Society of London. Series A, Mathematical and Physical Sciences* **293**, 341-348 (1979).
26 http://koski.ucdavis.edu/BRILLOUIN/horsehair/horsehair.html.
27 Koski K. J., Akhenblit P., McKiernan K. and Yarger J. L. Non-invasive determination of the complete elastic moduli of spider silks. *Nature Materials* **12**, 262-267 (2013).
28 Fioretto D., Caponi S. and Palombo F. Brillouin-Raman mapping of natural fibers with spectral moment analysis. *Biomedical Optics Express* **10**, 1469-1474 (2019).
29 Elsayad K. *et al.* Mechanical Properties of cellulose fibers measured by Brillouin spectroscopy. *Cellulose* **27**, 4209-4220 (2020).
30 Scarponi F. *et al.* High-Performance Versatile Setup for Simultaneous Brillouin-Raman Microspectroscopy. *Physical Review X* **7**, 031015 (2017).
31 Antonacci G., Foreman M. R., Paterson C. and Török P. Spectral broadening in Brillouin imaging. *Applied Physics Letters* **103**, 221105 (2013).
32 Caponi S., Fioretto D. and Mattarelli M. On the actual spatial resolution of Brillouin Imaging. *Optics Letters* **45**, 1063-1066 (2020).
33 Palombo F. *et al.* Chemico-mechanical imaging of Barrett's oesophagus. *Journal of Biophotonics* **9**, 694-700 (2016).
34 Palombo F., Madami M., Stone N. and Fioretto D. Mechanical mapping with chemical specificity by confocal Brillouin and Raman microscopy. *Analyst* **139**, 729-733 (2014).
35 Goin L. J., McKee W. H. and Kirk P. L. Human hair studies. Applications of the microdetermination of comparative density. *The Journal of Criminal Law, Criminology, and Police Science* **43**, 263-273 (1952).
36 Lee S. *et al.* Measurements of morphology and refractive indexes on human downy hairs using three-dimensional quantitative phase imaging. *Journal of Biomedical Optics* **20**, 111207 (2015).
37 Yasuda M., Sogabe A. and Noda A. Physical Properties of Human Hair 2. Evaluation of Human Hair Torsional Stress, and a Mechanism of Bending and Torsional Stress. *Journal of Society of Cosmetic Chemists of Japan* **36**, 262-272 (2002).
38 Edginton R. S., Green E. M., Winlove C. P., Fioretto D. and Palombo F. Dual scale biomechanics of extracellular matrix proteins probed by Brillouin scattering and quasistatic tensile testing. In *Proc. Photonics West BIOS Conf. - Biophysics, Biology and Biophotonics III: the Crossroads.* 105040J (2018).

39 Bailey M. *et al.* Viscoelastic properties of biopolymer hydrogels determined by Brillouin spectroscopy: A probe of tissue micromechanics. *Science Advances* **6**, eabc1937 (2020).
40 Tucker I. *et al.* Variation in tensile strength and microstructure of human hair in response to changes in humidity. PS 04 0109.